NEOPLASMA accepted, ahead of print manuscript
Cite article as https://doi.org/10.4149/neo_2025_250613N254

Running title: Salinomycin inhibits CCA by activating pyroptosis

Salinomycin promotes cell death via the activation of the ROS/NF-κB/NLRP3 pathway in cholangiocarcinoma

Xianfei Zhou, Fan Yang, Yisheng Ling, Luoshun Huang, Renwei Xing, Yong Lan, Yang Zhang*

Department of Hepatobiliary Surgery, Taizhou Municipal Hospital, Zhejiang, China

*Correspondence: waverain2023@163.com

Received June 13, 2025 / Accepted September 8, 2025

Salinomycin (Sal), an ionophore antibiotic, has shown promising anti-cancer activity in multiple cancers. In this study, we aimed to investigate the effect of Sal on the ROS/NF-κB/NLRP3 pathway in cholangiocarcinoma (CCA) *in vitro* and *in vivo*. We observed that Sal inhibited cell proliferation, migration, and invasion. Sal promoted an increase of Annexin-V positive cells in Huh-28 and RBE cells in a dose-dependent manner, which was efficiently inhibited by VX-765 (Caspase-1 inhibitor), while Sal-induced increase of ROS levels was partially inhibited by exposure to N-acetyl-L-cysteine (ROS scavenger). Moreover, Sal inhibited tumor growth in RBE tumor-bearing mice. The activation of Sal on the ROS/NF-κB/NLRP3 pathway was also identified in CCA cells and tumor tissues. Collectively, these results suggested that Sal activated the ROS/NF-κB/NLRP3 pathway to promote pyroptosis-induced cell death in CCA and suggest it may be a promising treatment strategy for anti-CCA.

Key words: salinomycin; cholangiocarcinoma; pyroptosis; NLRP3

Cholangiocarcinoma (CCA) is a malignant tumor originating from the epithelial cells of the bile ducts [1]. According to the anatomical differences in the location of the disease, CCA can be divided into intrahepatic cholangiocarcinoma (iCCA) and extrahepatic cholangiocarcinoma (eCCA), which is further subdivided into perihilar (pCCA) and distal (dCCA) cholangiocarcinoma [1, 2]. Surgical resection is the best treatment for CCA [3]. However, due to the lack of specific symptoms, the majority of patients are already in the progressive or advanced stage when diagnosed, missing the time of surgical treatment, and their 5-year survival rate is close to 5% [4]. Therefore, exploring new treatment strategies for CCA is an extremely urgent task for clinical workers.

At present, some research teams have actively carried out a large number of screening studies for anti-CCA drugs. Salinomycin (Sal), a natural carboxylic polyether ionophore first isolated from

Streptomyces albus in 1974, has emerged as a promising anticancer drug [5] to inhibit mitochondrial functions, subsequently leading to oxidative stress and injury, activation of AMPK, and suppression of mTOR [6]. A large number of studies have confirmed that Sal has the effect of inhibiting the growth of tumor cells and promoting apoptosis of tumor cells, including gastric cancer [7, 8], hepatocellular carcinoma [9], breast cancer [10], ovarian cancer [11], prostate cancer [12]. Additionally, a study by Yu et al. reported that Sal could inhibit the expression of adenylate-activated protein kinase family member 5 (ARK5) in RBE and Huh-28 cells, enhance the sensitivity of cholangiocarcinoma cells to doxorubicin chemotherapy, and thus reverse the process of epithelial-mesenchymal transition (EMT) of CCA cells [13]. However, the precise mechanism underlying the anti-cholangiocarcinogenic effect of Sal remains unclear. Therefore, further in-depth investigations are warranted.

Pyroptosis is a type of programmed, inflammatory cell death found after apoptosis and necrosis [14, 15], which mainly occurs through the cysteine-containing aspartate-specific proteases-1 (Caspase-1) pathway. Currently, as a form of programmed death, the occurrence of pyroptosis implies that the growth of tumor cells is inhibited, and the induction of tumor cell pyroptosis is an important pathway for anti-tumor immunity, which provides a new way of thinking for the prevention and treatment of malignant tumors [16-18]. Inflammasomes are multi-protein complexes assembled by intracellular pattern recognition receptors (PRR), which can recognize either pathogen-associated molecular pattern (PAMP) or damage-associated molecular pattern (DAMP) of host origin [19, 20]. Among them, the NLRP3 inflammasome, a cytoplasmic supramolecular complex, is involved in tumor pathogenesis [21, 22]. Furthermore, current literature suggests that the Toll-like receptor 4 (TLR4)/Myeloid differentiation factor-88 (MyD88)/nuclear factor-kappaB (NF-κB) pathway can activate NLRP3 inflammasome and then mediate cellular death [23]. The activation of TLR4 facilitates the binding to its primary adaptor protein, MyD88, through interactions between Toll/IL-1 receptor (TIR) domains. This process results in the phosphorylation of the NF-κB inhibitor IκB, causing the release of NF-κB from its inactive cytoplasmic state and its translocation to the nucleus, which in turn activates NLRP3 and triggers the release of pro-inflammatory mediators [23, 24]. Therefore, investigating whether Sal regulates cell death by modulating NLRP3/Caspase-1-mediated pyroptosis is one of the main focuses of CCA prevention and treatment research. In this study, we investigated the effect of Sal on cellular pyroptosis in CCA cells and the

molecular mechanism of its action, which provided an experimental basis for the investigation of the role of cellular pyroptosis in tumor cells and provided a new strategy for the treatment of CCA.

Materials and methods

Cell culture. The cholangiocarcinoma cell line Huh-28 was purchased from the Wanwu Biotechnology Co., Ltd (Hefei, China), and RBE cells were obtained from the Cellverse Bioscience Technology Co., Ltd. (Shanghai, China). All cells were cultured in Dulbecco's modified Eagle's medium (DMEM; Gibco, California, USA) supplemented with 10% fetal bovine serum (FBS, Gibco, USA) and 1% penicillin and streptomycin. The cell lines were cultured in a humidified atmosphere with 5% CO_2 at 37 °C.

Cell viability assay. Huh-28 and RBE cells were seeded in 96-well plates at a density of 5×10^3 cells/ well with normal medium overnight. Then, the different concentrations of Sal (20, 40, 60 μM, MedChemExpress, USA), Sal (20, 40, 60 μM)+Z-Vad-fmk (20 μM, Beyotime, China), VX-765 (20 μM, Topscience Co., Ltd, Shanghai, China), Sal (60 μM)+VX-765 (20 μM) were added in the corresponding group for incubating 24 h. After that, cells were incubated with 10 μl CCK-8 for 4 h at 37 °C. Then, the absorbance values at 450 nm of each well were measured by CMaxPlus Microplate Reader (Molecular Devices, USA).

Measurement of LDH, IL-1β, and IL-18 content. The cell supernatant of Sal (20, 40, 60 μM)-treated Huh-28 and RBE cells was collected and centrifuged. Then, the LDH level was determined by the LDH assay kit (Jiancheng, Nanjing, China). Also, the IL-1β and IL-18 contents were determined by commercial assay kits (#MM-0181H2, #MM-0139H1, Jiangsu Meimian Industrial Co., Ltd, China) according to the manufacturer's instructions.

EdU assay. Following the instructions in the BeyoClick™ EdU Cell Proliferation Kit with Alexa Fluor 594 (#C0078S, Beyotime, China), the Sal (20, 40, 60 μM)-treated Huh-28 and RBE cells in 12-well plates were stained with the 500 μl EdU solution. After 4 h, cells were fixed in 95% ethanol for 15 min, and nuclei were stained with DAPI. Finally, the images of cells were photographed under an inverted fluorescent microscope (Nikon, Japan).

Transwell assay. The migration and invasion abilities of Huh-28 and RBE cells treated with Sal were assessed through Transwell chambers (Corning, Inc., USA). For the cell invasion assay, the chambers were coated with 50 μl of 5 mg/ml Matrigel (BD, USA) at 37 °C overnight. Huh-28 and

RBE cells were pre-treated with Sal (20, 40, 60 μM) for 24 h. Subsequently, Huh-28 and RBE cells were seeded in upper chambers that were resuspended in a serum-free medium. The lower chamber was then filled with 600 μl of culture medium. After 24 h, the transwell chamber was taken out from the 24-well plate. Medium was discarded, and cells were washed with PBS twice. Next, the cells were incubated with 4% paraformaldehyde for 10 min and stained with 0.1% crystal violet for 30 min at room temperature. Images were captured under a light microscope at 200× magnification, and the cell numbers were quantified using ImageJ. Besides, the migration assay was carried out in something manner similar to the invasion assay, except using a Matrigel-coated membrane.

Cell cycle and apoptosis assays. Huh-28 and RBE cells were treated with the different concentrations of Sal (20, 40, 60 μM), VX-765 (20 μM), or Sal (60 μM)+VX-765 (20 μM) for 24 h. For cell cycle analysis, the Huh-28 and RBE cells were trypsinized using EDTA-free 0.25%. Following centrifugation, the supernatant was removed. Subsequently, the cells were resuspended with PBS and fixed with 70% ethanol overnight at -20 °C and stored at 4 °C. Following that, the cells were washed with PBS, incubated with RNase A (100 μg/ml) for 30 min, and stained with 10 μl propidium iodide (PI, 50 μg/ml, Sigma, USA) for 20 min at 37 °C. For the apoptosis assay, the collected Huh-28 and RBE cells were stained with 5 μl Annexin V-FITC and 10 μl PI in the dark for 15 min. Finally, the cell cycle distribution and apoptosis of Sal-treated Huh-28 and RBE cells were analyzed by using NovoCyte flow cytometer (Agilent, USA) and FlowJo (v10, https://www.flowjo.com/) software.

Transmission electron microscope (TEM). Huh-28 and RBE cells were seeded in a 6-well plate for overnight growth, then treated with Sal (60 μM) for 24 h. Then, the cells were washed and fixed with 2.5% glutaraldehyde in PBS for 4h. Subsequently, the cells were postfixed with 1% buffered osmium and stained with 1% potassium ferricyanide. After dehydration and embedding, the samples were maintained at 70 °C for 24 h. Finally, the digital images were taken using a transmission electron microscope (H-7650, Hitachi, Japan).

Hoechst 33242 staining. Huh-28 and RBE cells were seeded in 96-well plates at a density of 8×10^3 cells/well for 24 h before treatment with Sal (60 μM), VX-765 (20 μM), or Sal (60 μM)+VX-765 (20 μM). After incubation for 24 h, the Huh-28 and RBE cells were stained with 100 μl Hoechst 33342 (10 μg/ml, #C1025, Beyotime, China) for 15 min. Following Sal and VX-765 treatment, the Huh-28 and RBE cells were washed twice with PBS and then examined using a

fluorescence microscope.

ROS assay. Intracellular reactive oxygen species (ROS) levels were assessed by using 2′,7′-dichlorodihydrofluorescein diacetate (DCFH-DA) in a Reactive Oxygen Species Assay Kit (#S0033M, Beyotime, China). Briefly, the Huh-28 and RBE cells in a logarithmic growth phase were treated with Sal (20, 40, 60 μM), N-acetyl-L-cysteine (NAC, 1.5 mM, ROS inhibitor, Sigma-Aldrich), and Sal (60 μM)+NAC (1.5 mM) for 24 h. Cells were gently released and collected using trypsin and then were labeled with 3 μM DCFH-DA for 20 min and washed three times with free-serum DMEM. The level of ROS was determined by flow cytometry and analyzed by Flowjo software (BD Biosciences, CA, USA).

***In vivo* assay.** Six-week-old male BALB/c nude mice were purchased from Shanghai Jihui Laboratory Animal Breeding Co., Ltd (Shanghai, China) and housed under specific-pathogen-free (SPF) conditions. Approximately 1×10^6 RBE cells suspended in 100 μl PBS were subcutaneously injected into the right back of each nude mouse. Until the average tumor volume reached about 100 mm^3, the nude mice were randomly divided into 4 groups (6 mice/group). The Sal groups were treated with Sal (2, 4, 8 mg/kg) by gavage, and the model group was administered an equal volume of normal saline. Tumor size was measured every other day and calculated using the following formula: volume=(length × $width^2$)/2. After treatment for 21 days, all mice were sacrificed, and the tumor tissues were collected, weighed, and stored at -80 °C for Terminal deoxynucleotidyl transferase (TdT) dUTP Nick-End Labeling (Tunel) analysis and Western blot assays. Animal care and experimental procedures were approved by the Ethics Committee on the Animal Experimentation of Taizhou Municipal Hospital (Project No: TZMH-2023-268) and were conducted according to either the Canadian Council on Animal Care (CCAC) guidelines or the Guide for the Care and Use of Laboratory Animals (8^{th} edition, National Academies Press).

TUNEL analysis. The tumor tissues were fixed with 4% paraformaldehyde for 24 h at room temperature. Next, the fixed tissues were washed, dehydrated, embedded in paraffin, and sliced into 4 μm thick sections. Sections of tumor tissues were stained by the TUNEL method, using a One Step TUNEL Apoptosis Assay Kit (C1090, Beyotime, China), according to the instructions. The images of apoptosis of the sections were observed by fluorescence microscopy. Finally, the apoptosis rate was calculated as the number of apoptotic cells/total number of cells × 100%.

Western blot assay. The total proteins from Sal-treated Huh-28 and RBE cells and the tumor

tissues were extracted by using pre-colded RIPA buffer (#P0013B, Beyotime, China) with protease inhibitor cocktail (#CW2200S, JiangSu CoWin Biotech, China). The protein concentrations were quantified by a BCA Protein Assay (Beyotime, China). Protein samples (50 μg) were separated by sodium dodecyl sulphate-polyacrylamide gel electrophoresis (SDS-PAGE) and then transferred to polyvinylidene fluoride (PVDF) membranes, followed by being blocked with 5% skimmed milk. After that, the membranes were incubated with the primary antibodies anti-GSDMD-N (1:1000, #bs-14287R, Bioss Antibodies), anti-IL-1β (1:1000, #AF5103, Affinity), anti-ASC (1:1000, #DF6304, Affinity), anti-Cleaved Caspase-1 (1:1000, #AF4005, Affinity), anti-TLR4 (1:1000, #AF7017, Affinity), anti-MyD88 (1:1000, #AF5195, Affinity), anti-NF-κB p65 (1:1000, #AF2006, Affinity), anti-NLRP3 (1:1000, #DF7438, Affinity), and anti-GAPDH (1:10000, #10494-1-AP, Proteintech) at 4 °C overnight, followed by being incubated with horseradish peroxidase (HRP)-conjugated secondary antibody (1:6000, #7074, Cell Signaling Technology) at room temperature for 2 h. The blots were treated with an ECL detection kit (Beyotime, China), visualized using a chemiluminescence imaging system (#610020-9Q, Clinx Science Instruments), and quantified using the ImageJ software (National Institutes of Health, Bethesda, MD).

Statistical analysis. Data were revealed as the mean±standard deviation. All results were analyzed using SPSS 20.0 software (SPSS, Inc., Chicago, IL, USA). One-way analysis of variance (ANOVA) was applied for multiple comparisons. Differences between the two groups were assessed using Student's t-tests. P-value < 0.05 was considered statistically significant.

Results

Sal inhibited cell proliferation, migration, and invasion and promoted cell death in Huh-28 and RBE cells. The Huh-28 and RBE cells were incubated with 0, 20, 40, and 60 μM Sal for 24 h. Subsequently, the proliferation ability of Huh-28 and RBE cells was assessed by the CCK-8, LDH, and EdU assays. It was found that the Sal significantly decreased the cell viability of Huh-28 and RBE cells in a dose-dependent manner, as shown in Figure 1A. Compared to the control group, Sal treatment significantly increased the LDH release of Huh-28 and RBE cells (Figure 1B). Similarly, the EDU assay results also showed that Sal treatment significantly inhibited the proliferation of Huh-28 and RBE cells (Figure 1C). Furthermore, Sal treatment markedly reduced the migration and invasion of Huh-28 and RBE cells relative to the control group (Figure 1D). For further validation,

the results of flow cytometry showed that Sal treatment could induce G2/M phase arrest of Huh-28 and RBE cells (Figure 2A). Additionally, the results of flow cytometry showed that Sal treatment significantly increased population of Annexin-V^+ cells in Huh-28 and RBE cells compared with the control group (Figure 2B). Taken together, these results suggested that Sal treatment could suppress growth and migration and contribute to the cell death of Huh-28 and RBE cells.

Sal triggered non-apoptotic cell death and activated the NF-κB signaling pathway in Huh-28 and RBE cells. Compared to the control group, Sal treatment significantly decreased the cell viability of Huh-28 and RBE cells; however, z-Vad-fmk (Pan-caspase inhibitor) treatment did not reverse the reduction of cell viability induced by Sal in Huh-28 and RBE cells (Figure 3A). To further identify the type of cell death that also occurred in Sal-treated Huh-28 and RBE cells, TEM was employed to observe the ultra-structural changes in the cells, and the results revealed that cell swelling with large bubbles and multiple pores was found on the membranes of Sal-treated Huh-28 and RBE cells (Figure 3B). In addition, ELISA assays suggested a notable release of IL-1β and IL-18 cytokines into the culture mediums of Huh-28 and RBE cells treated with Sal (Figure 3C, 3D). More importantly, western blot assays displayed that the expressions of pyroptosis-associated proteins GSDMD-N, IL-1β, ASC, Cleaved caspase-1, TLR4, MyD88, NF-κB p65, and NLRP3 were markedly higher in Sal-treated Huh-28 and RBE cells compared with those in the control group (Figure 3E). Collectively, these results suggested that Sal-treated Huh-28 and RBE cells undergo pyroptosis to a certain extent.

Sal induced Caspase-1-mediated cell death in Huh-28 and RBE cells. Growing research suggests that caspase-1 is capable of proteolytically cleaving the precursors of inflammatory cytokines that consist of IL-1β and IL-18, along with GSDMD, towards mature and active forms, ultimately initiating cell pyroptotic death [21, 22]. In this study, a specific inhibitor of caspase-1 (VX-765) was also used. As a result, the CCK-8 assays showed that VX-765 significantly increased the cell viability of Sal-treated Huh-28 and RBE cells (Figure 4A). Moreover, the Hoechst 33242 staining and flow cytometry assays demonstrated that VX-765 could significantly decrease the percentage of apoptotic cells in Huh-28 and RBE cells (Figure 4B, 4C). Therefore, we could also conclude that Sal triggered cell death through the activation of Caspase-1 in Huh-28 and RBE cells.

Sal increases the intracellular ROS level in Huh-28 and RBE cells. As we know, ROS accumulation and the activation of the NF-κB pathway contribute to the activation of the NLRP3

inflammasome in cancer cells [24, 25]. Thus, we also investigated the intracellular ROS level in Sal-treated Huh-28 and RBE cells with or without N-acetyl-L-cysteine (NAC) treatment by using DCFH-DA. We found that Sal treatment markedly increased the intracellular ROS levels in Huh-28 and RBE cells (Figure 5A). Moreover, we found that NAC significantly reversed Sal-induced ROS levels in Huh-28 and RBE cells (Figure 5B). Notably, NAC significantly attenuated Sal-induced GSDMD-N, IL-1β, ASC, Cleaved caspase-1, NF-κB p65, and NLRP3 expressions in Huh-28 and RBE cells (Figure 5C). Collectively, these results suggested that Sal induces activation of the NF-κB/NLRP3 pathway in Huh-28 and RBE cells in a ROS-dependent manner.

Sal repressed tumor growth *in vivo* by up-regulating the NF-κB/NLRP3 pathway. To further investigate the effects of Sal on CCA in nude mice, we also established a subcutaneous tumor model. As expected, the results showed that Sal treatment significantly reduced tumor volume and weight *in vivo* (Figure 6A-6C). Furthermore, the TUNEL staining [26] demonstrated that a larger TUNEL-positive cell areas was observed in tumor tissues of RBE tumor-bearing mice with Sal treatment (Figure 6D). It was also found that Sal treatment increased protein expression levels of GSDMD-N, IL-1β, ASC, Cleaved Caspase-1, NF-κB p65, and NLRP3 in tumor tissues of nude mice (Figure 6E). Collectively, these findings suggest that Sal inhibited tumor growth *in vivo* may be associated with activation of the NF-κB/NLRP3 pathway.

Discussion

CCA is a tumor originating from the malignant proliferation of biliary epithelial cells and is the second most common hepatobiliary malignant tumor worldwide [2]. It is characterized by early invasion, poor prognosis, and high lethality, and in recent years, the incidence and mortality of CCA have been increasing year by year. Currently, the main treatment is surgery, but it still has a high recurrence rate and is resistant to chemotherapeutic drugs such as cisplatin [27]. Therefore, there is an urgent need to find effective treatments and drugs to improve the survival and prognosis of CCA patients. In recent years, the research on the antitumor effect of Sal has become a hot topic, which shows that Sal can activate the autophagy of cancer cells, destroy the microenvironment of tumor proliferation and differentiation, and strengthen its antitumor efficacy through the regulation of autophagy and the induction of apoptosis [28, 29]. In addition, Sal can regulate autophagy and induce apoptosis in cancer cells through the release of intracellular reactive oxygen species,

mitochondrial damage, endoplasmic reticulum stress, and inhibition of the Wnt/β-catenin signaling pathway, etc. [30, 31]. As a new type of antitumor drug, Sal has shown selective targeting and killing effects on a variety of tumor cells, but the mechanism of its action needs to be further researched. In this study, we also found that Sal treatment significantly inhibited cell proliferation, migration, and invasion of CCA cell lines Huh-28 and RBE cells *in vitro*. According to these findings, it was concluded that Sal could be a promising therapeutic agent for CCA patients, which may provide new therapeutic directions against CCA.

Uncontrolled cell growth and proliferation are features of tumor cells, and this uncontrolled proliferation is caused by anomalies in the cell cycle, and disruption of the cell cycle may contribute to tumorigenesis [32]. Apoptosis is a programmed cell death mechanism that plays a key role in preventing cancer [32, 33]. Tumor cell apoptosis evasion-tumor cells to become immortalized, is a fundamental trait in carcinogenesis, development, and metastasis. As a result, apoptosis is thought to be a significant therapeutic target for cancers. The study conducted by Zhang et al revealed that Sal inhibited cell growth and triggered endoplasmic reticulum (ER) stress to promote apoptosis in prostate cancer cells [34]. Additionally, Niwa et al. found that Sal induced cell cycle arrest in the G2/M phase and apoptosis in HepG2/C3a cells through up-regulation of CDKN1A and GADD45A and down-regulation of CCNB1 and CCNA2 [9]. Similarly, our study shows that Sal also induced cell cycle arrest in the G2/M phase and increased Annexin-V+ cells in Huh-28 and RBE cells. Interestingly, the promotion of Sal on cell death was significantly attenuated under VX-765 (Caspase-1 inhibitor) treatment. These data implicated that Sal significantly promoted cell death in Huh-28 and RBE cells might be associated with the activation of the cascade of the caspase-1 signaling pathway.

Recent research reveals that distinct programmed cell death procedures, such as apoptosis, ferroptosis, pyroptosis, and necroptosis, are important in the genesis and progression of CCA [35]. In the present study, the pan-caspase inhibitor, z-Vad-fmk, was used. The results of CCK-8 assays showed that Sal has an outstanding inhibitory effect on the cell viability of Huh-28 and RBE cells. However, it was also found in this study that the inhibitory effect on the cell viability of Sal was not reversed by using the pan-caspase inhibitor z-Vad-fmk treatment. This is due to the Sal also contributing to triggering non-apoptotic cell death in Huh-28 and RBE cells. Cellular pyroptosis is an inflammatory cell death mediated by caspase-1. Besides, NLRP3 activates caspase-1, and the

activated caspase-1 cuts the N-terminal sequence of GSDMD to become the pore-forming GSDMD-NT, which translocates to the cellular membrane structure to form the plasma membrane pore, resulting in disruption of the integrity of the cell membrane, thereby causing an increase in intracellular osmotic pressure and ultimately cell swelling and rupture [36]. In addition, activated caspase-1 can promote the activation and release of IL-1β and IL-18, which further promote the inflammatory response of the body [37, 38]. The fact that the z-VAD-FMK did not attenuate salinomycin-induced cell death suggests that apoptosis is a minor pathway and that the dominant form of cell death is likely caspase-1-mediated pyroptosis, as confirmed by our subsequent experiments. We found that the Sal elevated the expression of IL-1β and IL-18 in the cell-culture medium, as accompanied by an increase of protein expression levels in GSDMD-N, IL-1β, ASC, Cleaved caspase-1, TLR4, MyD88, NF-κB p65, and NLRP3 in Huh-28 and RBE cells. This evidence demonstrated that the up-regulation of cellular pyroptosis is also an important factor for Sal-induced therapy efficiency.

Reactive oxygen species (ROS) are related to cancer cell death, including apoptosis and pyroptosis. It has been reported that higher ROS levels can induce tumor cell death through a series of downstream pathways, the most important of which is the NF-κB/NLRP3 pathway [39]. Our study shows that Sal increases ROS production in Huh-28 and RBE cells. Interestingly, the ROS inhibitor NAC partially reversed this damage. Additionally, Sal can significantly inhibit the growth of subcutaneous tumors in mice by promoting cell apoptosis in the tumor tissues of RBE tumor-bearing mice. We also confirmed that Sal treatment increased the protein expression levels of GSDMD-N, IL-1β, ASC, Cleaved caspase-1, NF-κB p65, and NLRP3 in tumor tissues *in vivo*. Collectively, the *in vivo* investigation suggested that Sal treatment inhibited tumor growth be pyroptosis in RBE tumor-bearing mice.

In summary, we found that Sal can effectively inhibit the growth of CCA both *in vitro* and *in vivo* by targeting caspase-1-mediated cell death through the activation of the ROS/NF-κB/NLRP3 signaling cascade in Huh-28 and RBE cells. Most importantly, these results provide novel insights for Sal, used as a novel candidate for the treatment of CCA. However, this study had some limitations. Annexin-V/PI and Hoechst 33242 staining are not fully covered to discriminate apoptotic and pyroptotic cell death; additional accurate methods are needed to monitor the occurrence of pyroptosis in experimental cells. Besides, further functional studies are needed to

comprehensively evaluate the other pathways and targets influenced by Sal.

Acknowledgements: This study was supported by a grant from Zhejiang Provincial Natural Science Foundation of China (No. LQ23H160005) and Medical Health Science and Technology Project of Zhejiang Provincial Health Commission (No.2022KY1397).

References

[1] DE FRANCHIS V, PETRUNGARO S, PIZZICHINI E, CAMERINI S, CASELLA M et al. Cholangiocarcinoma Malignant Traits Are Promoted by Schwann Cells through TGFβ Signaling in a Model of Perineural Invasion. Cells 2024; 13: 366. https://doi.org/10.3390/cells13050366

[2] QURASHI M, VITHAYATHIL M, KHAN SA. Epidemiology of cholangiocarcinoma. Eur J Surg Oncol 2025; 51: 107064. https://doi.org/10.1016/j.ejso.2023.107064

[3] RIZVI S, KHAN SA, HALLEMEIER CL, KELLEY RK, GORES GJ. Cholangiocarcinoma - evolving concepts and therapeutic strategies. Nat Rev Clin Oncol 2018; 15: 95-111. https://doi.org/10.1038/nrclinonc.2017.157

[4] LI Y, YU J, ZHANG Y, PENG C, SONG Y et al. Advances in targeted therapy of cholangiocarcinoma. Ann Med 2024; 56: 2310196. https://doi.org/10.1080/07853890.2024.2310196

[5] JEDRZEJCZYK M, SULIK M, MIELCZAREK-PUTA M, LIM GY, PODSIAD M et al. Anticancer activity of salinomycin quaternary phosphonium salts. Eur J Med Chem 2025; 282: 117055. https://doi.org/10.1016/j.ejmech.2024.117055

[6] LI J, MIN Y. Pre-clinical evidence that salinomycin is active against retinoblastoma via inducing mitochondrial dysfunction, oxidative damage and AMPK activation. J Bioenerg Biomembr 2021; 53: 513-523. https://doi.org/10.1007/s10863-021-09915-2

[7] ZHANG Z, ZHAO J, MI Z, PANG Q, WANG A et al. Effects of salinomycin and 17- AAG on proliferation of human gastric cancer cells in vitro. Mol Med Rep 2017; 16: 1063-1070. https://doi.org/10.3892/mmr.2017.6735

[8] MAO Z, WU Y, ZHOU J, XING C. Salinomycin reduces epithelial-mesenchymal transition-mediated multidrug resistance by modifying long noncoding RNA HOTTIP expression in gastric cancer cells. Anticancer Drugs 2019; 30: 892-899. https://doi.org/10.1097/CAD.0000000000000786

[9] NIWA AM, SEMPREBON SC, D'EPIRO GFR, MARQUES LA, ZANETTI TA et al. Salinomycin induces cell cycle arrest and apoptosis and modulates hepatic cytochrome P450 mRNA expression in HepG2/C3a cells. Toxicol Mech Methods 2022; 32: 341-351. https://doi.org/10.1080/15376516.2021.2008570

[10] WANG H, ZHANG H, ZHU Y, WU Z, CUI C et al. Anticancer Mechanisms of Salinomycin in Breast Cancer and Its Clinical Applications. Front Oncol 2021; 11: 654428. https://doi.org/10.3389/fonc.2021.654428

[11] ZOU M, YIN X, ZHOU X, NIU X, WANG Y et al. Salinomycin-Loaded High-Density Lipoprotein Exerts Promising Anti-Ovarian Cancer Effects by Inhibiting

Epithelial-Mesenchymal Transition. Int J Nanomedicine 2022; 17: 4059-4071. https://doi.org/10.2147/IJN.S380598

[12] YU J, YANG Y, LI S, MENG P. Salinomycin triggers prostate cancer cell apoptosis by inducing oxidative and endoplasmic reticulum stress via suppressing Nrf2 signaling. Exp Ther Med 2021; 22: 946. https://doi.org/10.3892/etm.2021.10378

[13] YU Z, CHENG H, ZHU H, CAO M, LU C et al. Salinomycin enhances doxorubicin sensitivity through reversing the epithelial-mesenchymal transition of cholangiocarcinoma cells by regulating ARK5. Braz J Med Biol Res 2017; 50: e6147. https://doi.org/10.1590/1414-431X20176147

[14] FANG Y, TIAN S, PAN Y, LI W, WANG Q et al. Pyroptosis: A new frontier in cancer. Biomed Pharmacother 2020; 121: 109595. https://doi.org/10.1016/j.biopha.2019.109595

[15] YANG F, BETTADAPURA SN, SMELTZER MS, ZHU H, WANG S. Pyroptosis and pyroptosis-inducing cancer drugs. Acta Pharmacol Sin 2022; 43: 2462-2473. https://doi.org/10.1038/s41401-022-00887-6

[16] TONG X, TANG R, XIAO M, XU J, WANG W et al. Targeting cell death pathways for cancer therapy: recent developments in necroptosis, pyroptosis, ferroptosis, and cuproptosis research. J Hematol Oncol 2022; 15: 174. https://doi.org/10.1186/s13045-022-01392-3

[17] CAI J, YI M, TAN Y, LI X, LI G et al. Natural product triptolide induces GSDME-mediated pyroptosis in head and neck cancer through suppressing mitochondrial hexokinase-II. J Exp Clin Cancer Res 2021; 40: 190. https://doi.org/10.1186/s13046-021-01995-7

[18] WU Y, PI D, ZHOU S, YI Z, DONG Y et al. Ginsenoside Rh3 induces pyroptosis and ferroptosis through the Stat3/p53/NRF2 axis in colorectal cancer cells. Acta Biochim Biophys Sin (Shanghai) 2023; 55: 587-600. https://doi.org/10.3724/abbs.2023068

[19] Li P, CHANG M. Roles of PRR-Mediated Signaling Pathways in the Regulation of Oxidative Stress and Inflammatory Diseases. Int J Mol Sci 2021 19; 22: 7688. https://doi.org/10.3390/ijms22147688

[20] PANDEY A, LI Z, GAUTAM M, GHOSH A, MAN SM. Molecular mechanisms of emerging inflammasome complexes and their activation and signaling in inflammation and pyroptosis. Immunol Rev 2025; 329: e13406. https://doi.org/10.1111/imr.13406

[21] TENGESDAL IW, DINARELLO CA, MARCHETTI C. NLRP3 and cancer: Pathogenesis and therapeutic opportunities. Pharmacol Ther 2023; 251: 108545. https://doi.org/10.1016/j.pharmthera.2023.108545

[22] WEN J, XUAN B, LIU Y, WANG L, HE L et al. NLRP3 inflammasome-induced pyroptosis in digestive system tumors. Front Immunol 2023; 14: 1074606. https://doi.org/10.3389/fimmu.2023.1074606

[23] YANG J, ZHANG M, LUO Y, XU F, GAO F et al. Protopine ameliorates OVA-induced asthma through modulating TLR4/MyD88/NF-κB pathway and NLRP3 inflammasome-mediated pyroptosis. Phytomedicine 2024; 126: 155410. https://doi.org/10.1016/j.phymed.2024.155410

[24] CHEN M, HU C, YANG L, GUO Q, LIANG Y et al. Saikosaponin-D induces the pyroptosis of lung cancer by increasing ROS and activating the NF-κB/NLRP3/caspase-1/GSDMD pathway. J Biochem Mol Toxicol 2023; 37: e23444. https://doi.org/10.1002/jbt.23444

[25] LI L, XU T, QI X. Balanced regulation of ROS production and inflammasome activation in preventing early development of colorectal cancer. Immunol Rev 2025; 329: e13417. https://doi.org/10.1111/imr.13417

[26] WANG S, LIU Y, ZHANG L, SUN Z. Methods for monitoring cancer cell pyroptosis. Cancer Biol Med 2021; 19: 398-414. https://doi.org/10.20892/j.issn.2095-3941.2021.0504
[27] SHI X, HU Z, BAI S, ZONG C, XUE H et al. YBX1 promotes stemness and cisplatin insensitivity in intrahepatic cholangiocarcinoma via the AKT/β-catenin axis. J Gene Med 2024; 26: e3689. https://doi.org/10.1002/jgm.3689
[28] KIM SH, CHOI YJ, KIM KY, YU SN, SEO YK et al. Salinomycin simultaneously induces apoptosis and autophagy through generation of reactive oxygen species in osteosarcoma U2OS cells. Biochem Biophys Res Commun 2016; 473: 607-613. https://doi.org/10.1016/j.bbrc.2016.03.132
[29] JIANG J, LI H, QAED E, ZHANG J, SONG Y et al. Salinomycin, as an autophagy modulator- a new avenue to anticancer: a review. J Exp Clin Cancer Res 2018; 37: 26. https://doi.org/10.1186/s13046-018-0680-z
[30] XIPELL E, GONZALEZ-HUARRIZ M, MARTINEZ DE IRUJO JJ, GARCIA-GARZON A, LANG FF et al. Salinomycin induced ROS results in abortive autophagy and leads to regulated necrosis in glioblastoma. Oncotarget 2016; 7: 30626-30641. https://doi.org/10.18632/oncotarget.8905
[31] LIU Q, SUN J, LUO Q, JU Y, SONG G. Salinomycin Suppresses Tumorigenicity of Liver Cancer Stem Cells and Wnt/Beta-catenin Signaling. Curr Stem Cell Res Ther 2021; 16: 630-637. https://doi.org/10.2174/1574888X15666200123121225
[32] SUN Y, LIU Y, MA X, HU H. The Influence of Cell Cycle Regulation on Chemotherapy. Int J Mol Sci 2021; 22: 6923. https://doi.org/10.3390/ijms22136923
[33] DAS S, SHUKLA N, SINGH SS, KUSHWAHA S, SHRIVASTAVA R. Mechanism of interaction between autophagy and apoptosis in cancer. Apoptosis 2021; 26: 512-533. https://doi.org/10.1007/s10495-021-01687-9
[34] ZHANG Y, LI F, LIU L, JIANG H, HU H et al. Salinomycin triggers endoplasmic reticulum stress through ATP2A3 upregulation in PC-3 cells. BMC Cancer 2019; 19: 381. https://doi.org/10.1186/s12885-019-5590-8
[35] SCIMECA M, ROVELLA V, PALUMBO V, SCOOLI MP, BONFIGLIO R et al. Programmed Cell Death Pathways in Cholangiocarcinoma: Opportunities for Targeted Therapy. Cancers (Basel) 2023; 15: 3638. https://doi.org/10.3390/cancers15143638
[36] HE WT, WAN H, HU L, CHEN P, WANG X et al. Gasdermin D is an executor of pyroptosis and required for interleukin-1β secretion. Cell Res 2015; 25: 1285-1298. https://doi.org/10.1038/cr.2015.139
[37] HUANG Y, XU W, ZHOU R. NLRP3 inflammasome activation and cell death. Cell Mol Immunol 2021; 18: 2114-2127. https://doi.org/10.1038/s41423-021-00740-6
[38] XU J, NUNEZ G. The NLRP3 inflammasome: activation and regulation. Trends Biochem Sci 2023; 48: 331-344. https://doi.org/10.1016/j.tibs.2022.10.002
[39] TENG JF, MEI QB, ZHOU XG, TANG Y, XIONG R et al. Polyphyllin VI Induces Caspase-1-Mediated Pyroptosis via the Induction of ROS/NF-κB/NLRP3/GSDMD Signal Axis in Non-Small Cell Lung Cancer. Cancers (Basel) 2020; 12: 193. https://doi.org/10.3390/cancers12010193

Figure Legends

Figure 1. Effect of Sal on cell proliferation, migration, and invasion in Huh-28 and RBE cells. A) CCK-8, B) ELISA, and C) EdU assays (scale bar, 100 μm) were performed to assess the proliferative capacity and LDH activity in Huh-28 and RBE cells after Sal treatment. D) Transwell assay was conducted to analyze the migration and invasion abilities of Huh-28 and RBE cells after Sal treatment. Scale bar, 100 μm. *$p < 0.05$, **$p < 0.01$ vs. Control group

Figure 2. Effect of Sal on cell cycle and Annexin-V+ cells in Huh-28 and RBE cells. A) Cell cycle progression and B) Annexin-V+ cells were examined by flow cytometry *$p < 0.05$, **$p < 0.01$ vs. Control group.

Figure 3. Effect of Sal on non-apoptotic cell death in Huh-28 and RBE cells. A) Inhibitory action of z-Vad-fmk on the cell viability in Sal-treated Huh-28 and RBE cells. B) Ultra-structural changes in the Sal-treated Huh-28 and RBE cells were detected by TEM. Pyroptotic bodies (red arrows) were found. Images were captured at 10,000× magnification. Scale bar, 2 μm. C) Interleukin-1β (IL-1β) and D) interleukin-18 (IL-18) levels in culture supernatants from Sal-treated Huh-28 and RBE cells were assessed by ELISA. E) Pyroptosis and TLR4/MyD88/ NF-κB p65-associated proteins were analyzed by Western blot assays. *$p < 0.05$, **$p < 0.01$ vs. Control group

Figure 4. Effect of Sal on Caspase-1-mediated Annexin-V+ in Huh-28 and RBE cells. A) CCK-8 assays of Huh-28 and RBE cells after treatment with Sal (60 μM) for 24 h in the presence of VX-765 (20 μM, Caspase-1 inhibitor). B) Hoechst 33242 staining (Scale bar, 100 μm) and C) flow cytometry assays were performed to measure Annexin-V+ cells in Huh-28 and RBE cells treated with Sal 532 (60 μM) and VX-765 (20 μM) alone or in combination. **$p < 0.01$ vs. SAL group

Figure 5. Effect of Sal on the intracellular reactive oxygen species (ROS) levels in Huh-28 and RBE cells. A) The intracellular ROS levels of Huh-28 and RBE cells treated with a series of concentrations of Sal (20, 40, 60 μM) were measured by using flow cytometry assays. B) The intracellular ROS levels of Huh-28 and RBE cells treated with Sal (60 μM) and N-acetyl-L-cysteine (NAC, 1.5 mM, ROS inhibitor) alone or in combination were detected by flow cytometry. C) Pyroptosis-associated proteins, NF-kB p65, and NLRP3 expressions were determined via Western

blot. **p <0.01 vs. Control and SAL groups

Figure 6. Effect of Sal on the tumor growth of RBE tumor-bearing mice *in vivo*. A) Balb/c nude mice were subcutaneously implanted with RBE cells, and treated with Sal (2, 4, 8 mg/kg) for 21 days, and the tumor tissues were collected and photographed. B) Tumor volume and C) weight of Sal-treated mice were recorded. D) TUNEL staining was used for analyzing the cell death level in the tumor tissues of Sal-treated mice. Scale bar, 50 μm. E) Western blot was employed for analyzing the expression of pyroptosis-associated proteins, NF-kB p65, and NLRP3 in tumor tissues of Sal-treated mice. *p < 0.05, **p < 0.01 vs. Model group.

Fig. 1 [Download full resolution image]

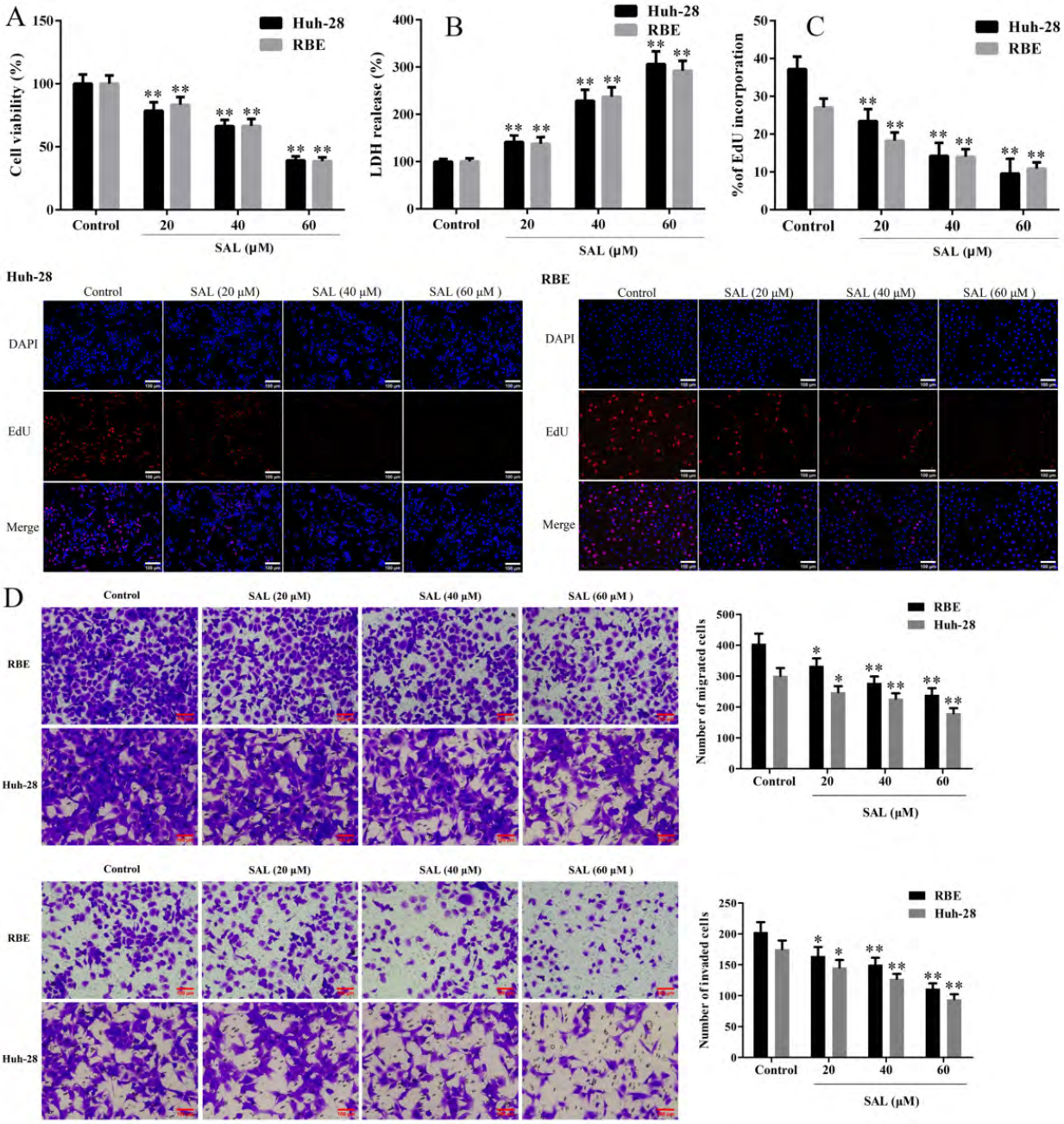

Fig. 2 [Download full resolution image]

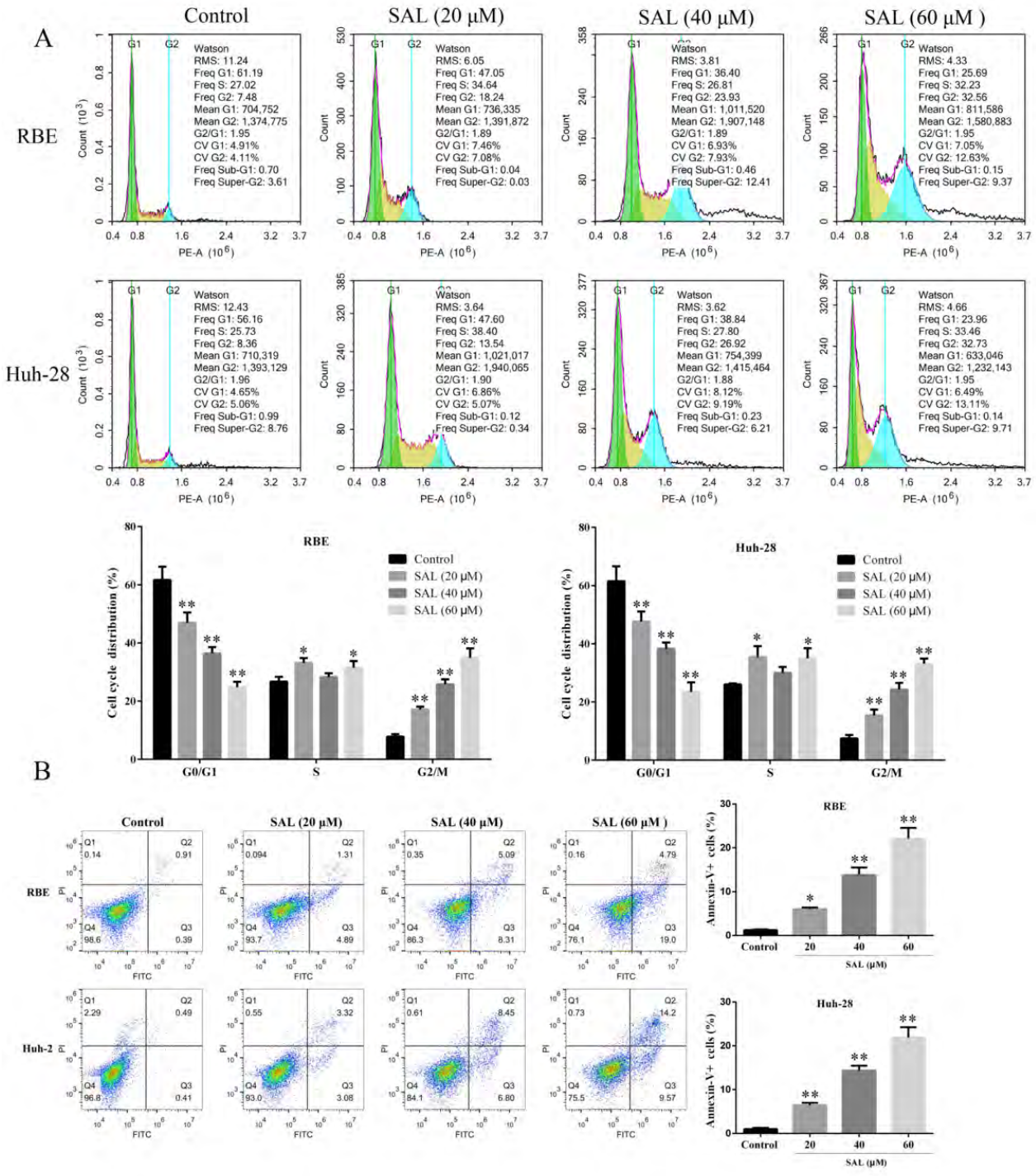

Fig. 3 [Download full resolution image]

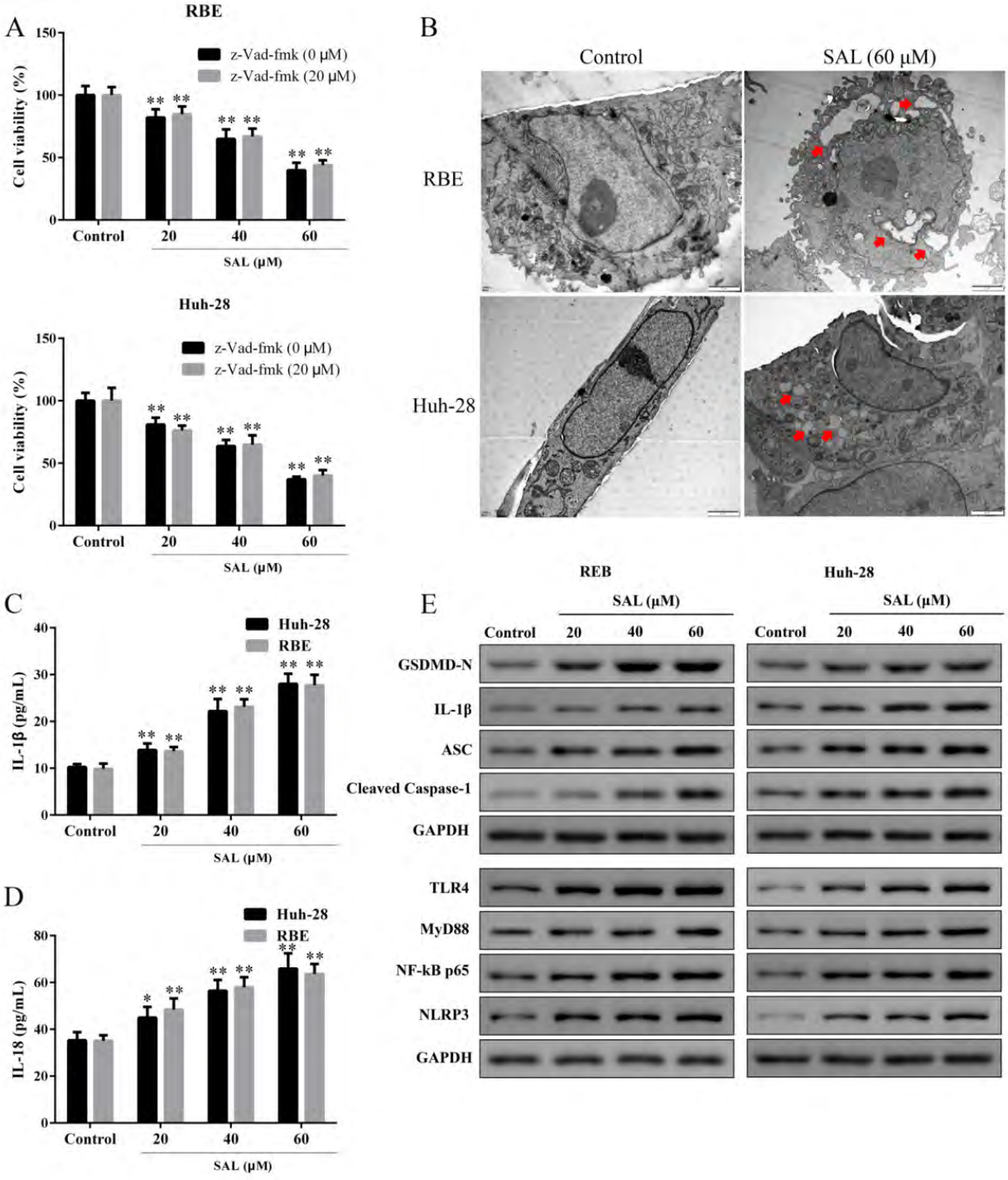

Fig. 4 [Download full resolution image]

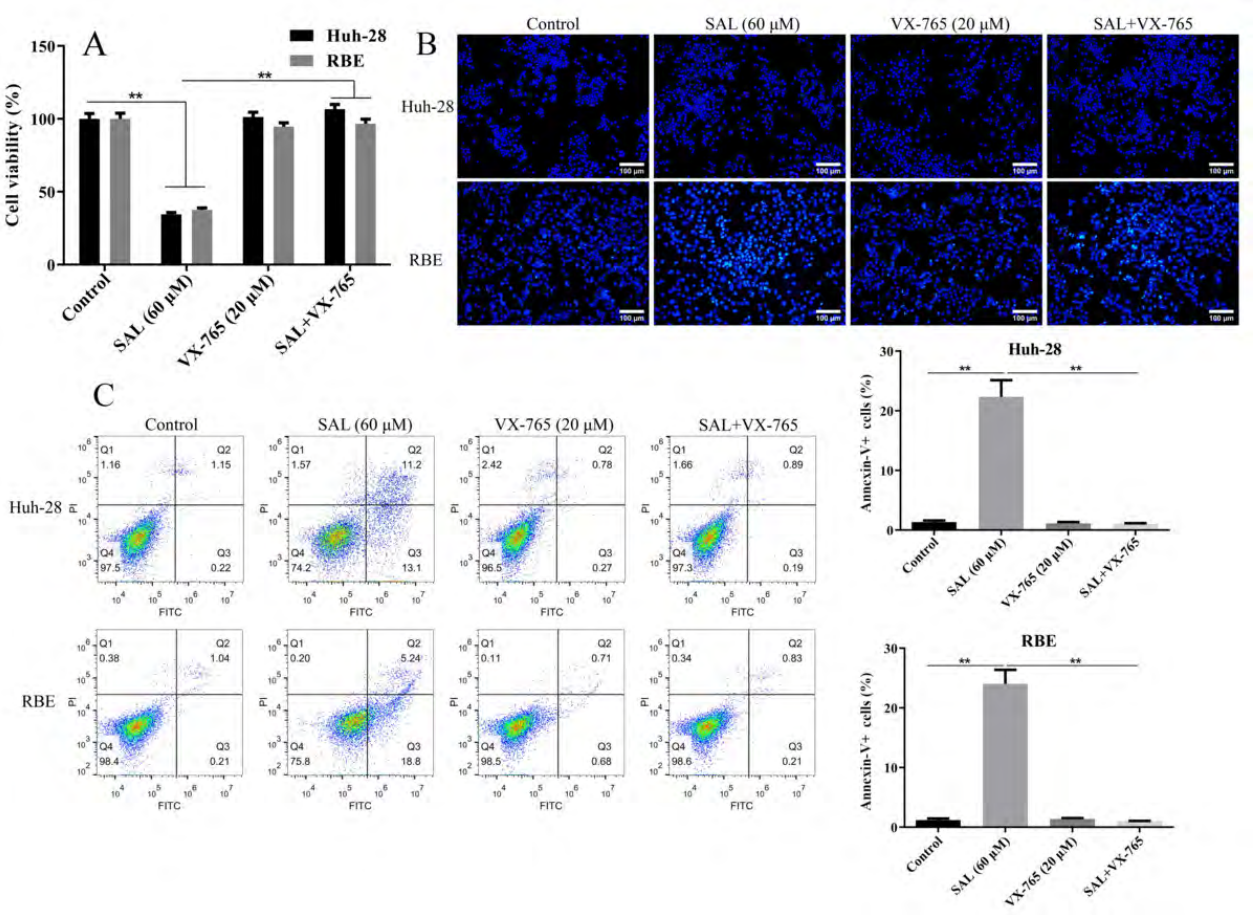

Fig. 5 Download full resolution image

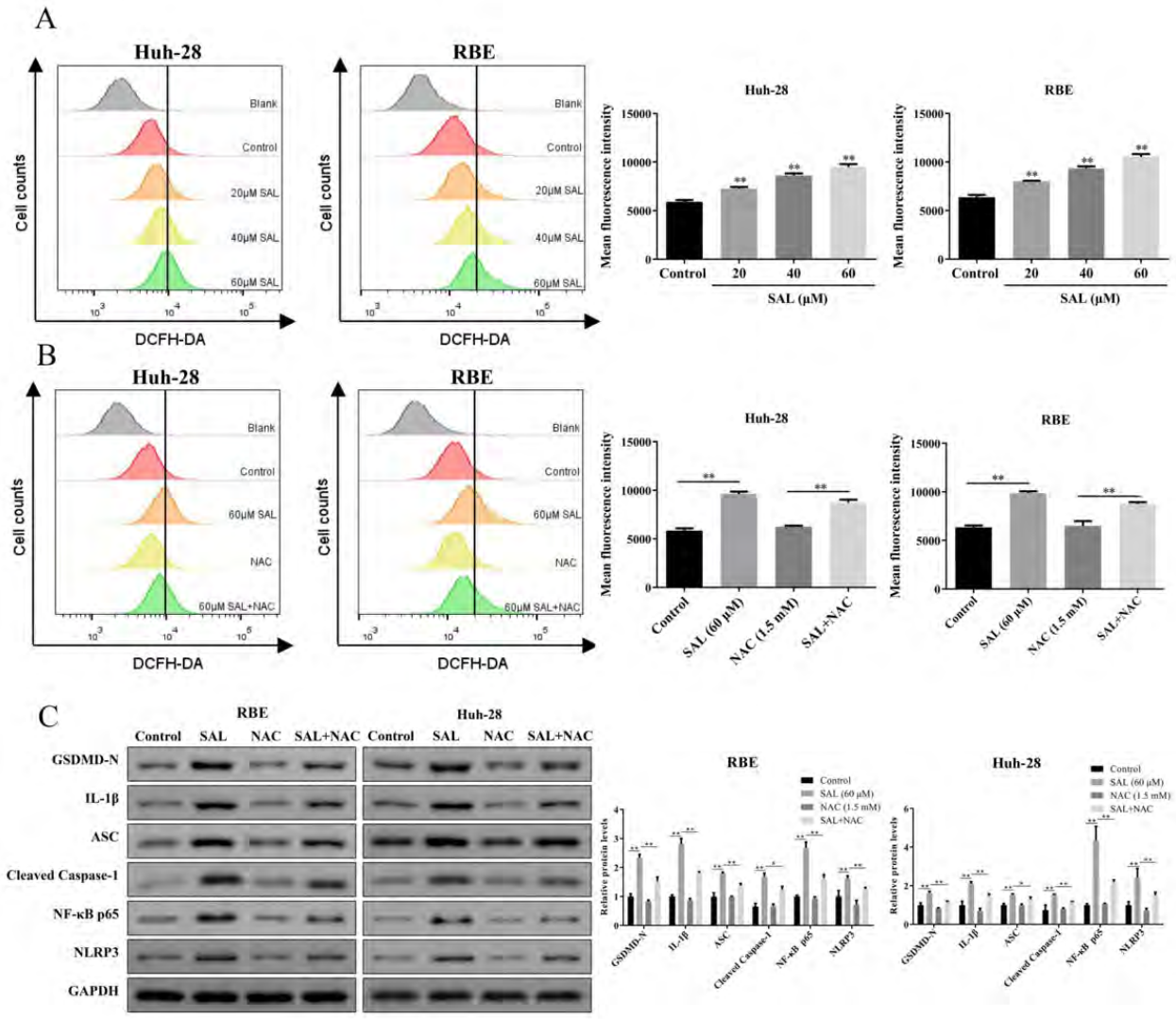

Fig. 6 Download full resolution image